Available online at www.sciencedirect.com
SCIENCE DIRECT®
ELSEVIER
International Journal of Solids and Structures 42 (2005) 5021–5035
INTERNATIONAL JOURNAL OF SOLIDS and STRUCTURES
www.elsevier.com/locate/ijsolstr

Dynamic behavior of long-span box girder bridges subjected to moving loads: Numerical analysis and experimental verification

Sang-Youl Lee [a,1], Sung-Soon Yhim [b,*]

[a] *Department of Structural Mechanics, University of Granada, Politécnico de Fuentenueva, 18071 Granada, Spain*
[b] *Department of Civil Engineering, University of Seoul, 90 Junneoung-Dong, Dongdaemoon-Gu, Seoul 130-743, South Korea*

Received 9 September 2004; received in revised form 12 February 2005
Available online 21 March 2005

Abstract

In this study we conducted three-dimensional dynamic analyses of long-span box girder bridges subjected to moving loads, using four-node Lagrangian and Hermite finite elements. In finite element formulation, a 6×6 transformation matrix is derived to transform the system element matrices before assembly. The usual 5 degrees of freedom per node are appended with an additional drilling degree of freedom in order to fit the transformation. The numerical results show good agreement with the experimental data from an existing two-span prestressed concrete box girder bridge under travelling vehicles. Parametric studies are focused on the various effects of moving loads on the dynamic behavior for different locations on the cross-section of box girder bridges.

Keywords: Moving loads; Folded plate; Finite element method; Dynamic response; Drilling degree of freedom; Experimental data

1. Introduction

The trend of urban expansion accelerated by rapid industrialization has indirectly affected the transportation vehicles causing a steady increase in their sizes. In order to achieve higher efficiency rates, increasingly larger transportation vehicles are manufactured. This situation however, has raised the major issue of the capabilities of current bridges in meeting the prevalent demands. Specifically, bridges are subjected

* Corresponding author. Tel.: +82 2 2210 2535.
E-mail addresses: leesy@mit.edu (S.-Y. Lee), yhimss@uos.ac.kr (S.-S. Yhim).
[1] Tel.: +82 222943330; fax: +82 24009134.

0020-7683/$ - see front matter © 2005 Elsevier Ltd. All rights reserved.
doi:10.1016/j.ijsolstr.2005.02.020

to larger loads than they were originally designed for, which accelerates their deterioration and eventually, their failure, signaling the need for bridges with higher capacities. Bridges with closed sections have many advantages over the traditional I-girder bridges, as they offer higher bending and torsional stiffness. For these reasons, box girder bridges have gained popularity as can be seen in their widespread usage in recent constructions.

Theoretical and experimental studies of the dynamic behavior of bridges subject to moving vehicles have been conducted for more than 100 years. Theoretically, the problem of a moving load was first tackled for the case in which the beam mass was considered small in comparison with the mass of a single, constant load. The original approximate solution was proposed by Willis (1849) and Stokes (1849), one of the early experimenters in the field. In the 20th century, vibration of beam as a result of moving loads were studied in idealized vibrations of the railway bridges by Timoshenko (1922), Jeffcott (1929), Lowan (1935), and Looney (1958). Biggs (1959) conducted several field investigations, and theoretical studies related to the dynamic behavior of bridges using one idealized beam and considering the basic vibration mode and viscous damping. Veletsos and Huang (1970) analyzed a three-span continuous bridge, studying effects of various parameters such as the vehicle velocity, axle spacing, weight ratio of the vehicle and the bridge, and dynamic characteristics of the vehicles. Recently, various researches have been conducted on vehicle-induced vibrations of bridges (Chatterjee et al., 1994; Chu et al., 1986; Hwang and Nowark, 1991; Thambiratnam et al., 2000; Yang and Yau, 1997).

However, all these works are limited, since they analyze only structures that are idealized by a beam member. In the case of box girders, the simplified analysis with idealized beam elements is based on the assumption that the cross-section of the box girder subjected to loads necessarily sustains its original shape. This simplified analysis cannot definitely specify the structural behavior at the cross-section of the box girder. Cheung (1969) introduced the finite strip method (FSM) for the analysis of folded prismatic plates and box girders under the effect of moving mass. In general, if a plate structure has constant cross-section and its end support condition does not change transversely, the finite strip method can accurately describe the kinematic behavior of a box girder bridge (Maleki, 1991; Senthilvasan et al., 2002). However, if the structure has irregularities, e.g. a rectangular plate with openings, the FSM is no longer applicable (Cheung et al., 1996). In addition, when the load is moving along the bridge, FSM cannot obtain accurate results because the load application point must be taken as a node and a dense mesh is required around this point (Cheung et al., 1996). In contrast, the finite element method (FEM) adopted in this study uses 6-DOF per node including a drilling DOF and thus can yield more accurate results than the FSM for dynamic analysis of the bridges under moving loads. Bathe (1996) and Zienkiewicz and Taylors (2000) presented FEM using a flat shell element, which can be applied directly to folded plate structures. However, they do not consider the dynamic effects of moving loads. In this paper, the existing FEM using flat shell elements is further extended to study the dynamic response of continuous box girder bridges subjected to moving loads. The numerical results are verified by comparing them with measurement data obtained from experimental works on a prestressed concrete box girder bridge.

2. Governing equations

The unfolded flat shell element with local 5-DOF per node can be obtained by superimposing the plate bending on the plane stress behavior (Bathe, 1996). Fig. 1 shows a coordinate system and the components of displacement and rotation. In Fig. 1, x, y, and z are directions for the local coordinate system, $u(x,y,t)$ and $v(x,y,t)$ are displacements for the plane stress behavior at the point x, y and at time t. Moreover, $w(x,y,t)$, $\theta_x(x,y,t)$ and $\theta_y(x,y,t)$ are vertical displacement and rotations along x and y axes for the dynamic plate bending behavior, respectively. The governing equations for the plane stress behavior are given by

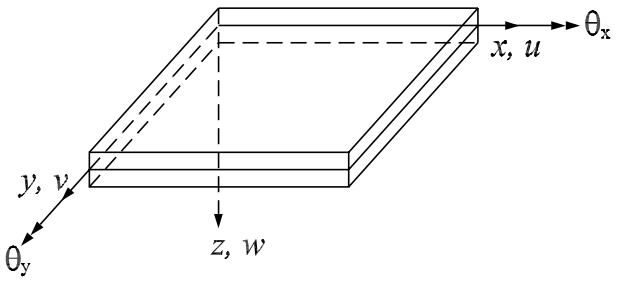

Fig. 1. Coordinates, displacements and rotations of a plate element in the global coordinates.

$$\frac{E}{1-v^2}\left(\frac{\partial^2 u(x,y,t)}{\partial x^2}+\frac{1+v}{2}\frac{\partial^2 v(x,y,t)}{\partial x\partial y}+\frac{1-v}{2}\frac{\partial^2 u(x,y,t)}{\partial y^2}\right)=f_x(x,y,t)-\mu\frac{\partial^2 u(x,y,t)}{\partial t^2}, \tag{1}$$

$$\frac{E}{1-v^2}\left(\frac{1-v}{2}\frac{\partial^2 v(x,y,t)}{\partial x^2}+\frac{1+v}{2}\frac{\partial^2 u(x,y,t)}{\partial x\partial y}+\frac{\partial^2 v(x,y,t)}{\partial y^2}\right)=f_y(x,y,t)-\mu\frac{\partial^2 v(x,y,t)}{\partial t^2}, \tag{2}$$

where E and v denote the moduli of elasticity and Poisson's ratio, $f_x(x,y,t)$ and $f_y(x,y,t)$ are in-plane loads per unit area for x, y-directions, and μ is the mass density, respectively. The governing equation for plate bending behaviors is written as

$$\frac{Eh^3}{12(1-v^2)}\left(\frac{\partial^4 w(x,y,t)}{\partial x^4}+2\frac{\partial^4 w(x,y,t)}{\partial x^2\partial y^2}+\frac{\partial^4 w(x,y,t)}{\partial y^4}\right)=f_z(x,y,t)-\mu\frac{\partial^2 w(x,y,t)}{\partial t^2}, \tag{3}$$

where h is the plate thickness and $f_z(x,y,t)$ is the vertical load per unit area of the plate.

3. Finite element method

The FEM for analyzing unfolded plates reviewed in this study is derived from the formulation of Bathe (1996). To analyze folded structures, we introduce a displacement finite element model using nonconforming elements of 6-DOF including the modified drilling degree of freedom per node.

3.1. Unfolded flat shell element

In FEM, the governing equations described by Eqs. (1)–(3) require the Lagrange interpolation of (u_j, v_j) and Hermite interpolation of $(w_j, \theta_{xj}, \theta_{yj})$ at a node j of plate element. The displacements at any point within the element can be expressed as

$$\begin{Bmatrix} u \\ v \end{Bmatrix}=\sum_{j=1}^{4}\Psi_j[I_2]\begin{Bmatrix} u_j \\ v_j \end{Bmatrix} \quad \text{and} \quad \begin{Bmatrix} w \\ \theta_x \\ \theta_y \end{Bmatrix}=\sum_{j=1}^{4}\begin{bmatrix} \Phi_j & \Phi_j & \Phi_j \\ \Phi_{j,x} & \Phi_{j,x} & \Phi_{j,x} \\ \Phi_{j,y} & \Phi_{j,y} & \Phi_{j,y} \end{bmatrix}\begin{Bmatrix} w_j \\ \theta_{xj} \\ \theta_{yj} \end{Bmatrix}, \tag{4}$$

where $[I_2]$ is a 2×2 identity matrix, Ψ_j are Lagrange interpolation functions, and Φ_j, $\Phi_{j,x}$ and $\Phi_{j,y}$ are the Hermite interpolation functions, and their first derivatives, respectively. The element stiffness matrix $[K]_e$ of the unfolded plate element can be calculated by Eq. (5).

$$[K]_e=\int_0^a\int_0^b [B]^T[D][B]\,dx\,dy, \tag{5}$$

where a and b are the dimensions of a rectangular plate, $[B]$ is the strain–displacement matrix, and $[D]$ is a constitutive matrix. Alternatively, Eq. (5) can be rewritten in the natural coordinates (ξ,η) as

$$[K]_r = \int_{-1}^{1}\int_{-1}^{1} [\overline{B}]^{\mathrm{T}}[D][\overline{B}] \mid J \mid \mathrm{d}\xi\,\mathrm{d}\eta, \tag{6}$$

where $[K]_r$ is an element stiffness matrix in the natural coordinates, and $|J|$ is a determinant of Jacobian matrix. The strain–displacement matrix $[\overline{B}]$ in the coordinates (ξ,η) is given by

$$[\overline{B}] = \sum_{j=1}^{4} \begin{bmatrix} \Psi_{j,\xi} & 0 & 0 & 0 & 0 \\ 0 & \Psi_{j,\eta} & 0 & 0 & 0 \\ \Psi_{j,\xi} & \Psi_{j,\eta} & 0 & 0 & 0 \\ 0 & 0 & \Phi_{j,\xi\xi} & \Phi_{j,\xi\xi} & \Phi_{j,\xi\xi} \\ 0 & 0 & \Phi_{j,\eta\eta} & \Phi_{j,\eta\eta} & \Phi_{j,\eta\eta} \\ 0 & 0 & \Phi_{j,\xi\eta} & \Phi_{j,\xi\eta} & \Phi_{j,\xi\eta} \end{bmatrix}. \tag{7}$$

The mass matrix of the unfolded flat shell element is given by

$$[M]_{\mathrm{e}} = \int_0^a \int_0^b \mu[H]^{\mathrm{T}}[H]\,\mathrm{d}x\,\mathrm{d}y = \int_{-1}^{1}\int_{-1}^{1} \mu[\overline{H}]^{\mathrm{T}}[\overline{H}] \mid J \mid \mathrm{d}\xi\,\mathrm{d}\eta, \tag{8}$$

where $[H]$ is a matrix consisting of Lagrange and Hermite interpolation functions.

3.2. Folded flat shell element

It is known that the global stiffness matrix is singular or ill-conditioned because of the null diagonal terms due to the drilling DOF (in-plane rotation, θ_z) in the transformed element stiffness matrix. As a result, it is difficult to solve the global equilibrium equations. The θ_z at a node is not measured and does not contribute to the strain energy stored in the element. To resolve this problem in a finite element analysis, Zienkeiwicz and Taylor defined a fictious set of rotation stiffness coefficients in all element whether co-planar or not. However, it has somewhat complicated formulations for different element shapes. On the other hand, we artificially insert an in-plane rotation angle or alternatively rotational stiffness coefficients without such assumed formulation. In our analysis, we add an appropriate sixth drilling DOF to the existing 5-DOF system, as suggested by Lee et al. (2002). The appropriate coefficient is determined by static and dynamic analyses in Section 4.1.

The deformations of each element expressed in the local coordinate can be transformed to the global coordinates by using the following transformation relationship (see Fig. 2):

$$\begin{Bmatrix} u \\ v \\ w \\ \theta_x \\ \theta_y \\ \theta_z \end{Bmatrix} = \begin{bmatrix} l_{x'x} & l_{x'y} & l_{x'z} & 0 & 0 & 0 \\ l_{y'x} & l_{y'y} & l_{y'z} & 0 & 0 & 0 \\ l_{z'x} & l_{z'y} & l_{z'z} & 0 & 0 & 0 \\ 0 & 0 & 0 & l_{y'y} & -l_{y'x} & l_{y'z} \\ 0 & 0 & 0 & -l_{x'y} & l_{x'x} & -l_{x'z} \\ 0 & 0 & 0 & l_{z'y} & -l_{z'x} & l_{z'z} \end{bmatrix} \begin{Bmatrix} u' \\ v' \\ w' \\ \theta'_x \\ \theta'_y \\ \theta'_z \end{Bmatrix} \tag{9}$$

where, l_{ij} are the direction cosines between the global and local coordinates, or, briefly,

$$\{u\} = [T]\{u'\} \tag{10}$$

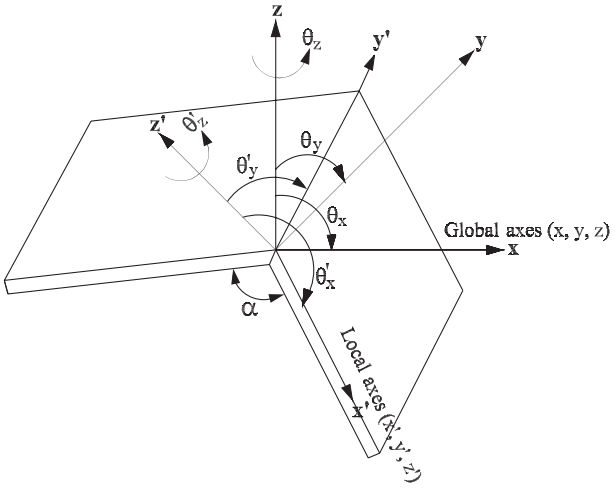

Fig. 2. Coordinate transformations for a folded plate element.

and $[T]$ is the transformation matrix. The primed notations in Eqs. (9) and (10) are used to denote the deformations in local coordinates. The global stiffness matrix is then expressed as,

$$[\overline{K}] = [\overline{T}]^{\mathrm{T}}[\overline{K}_s][\overline{T}], \tag{11}$$

where

$$[\overline{T}] = \begin{bmatrix} [T] & 0 & 0 & 0 \\ 0 & [T] & 0 & 0 \\ 0 & 0 & [T] & 0 \\ 0 & 0 & 0 & [T] \end{bmatrix}_{24\times 24} \qquad [\overline{K}_s] = \begin{bmatrix} [K]_r & 0 \\ 0 & [K]_d \end{bmatrix}_{24\times 24}. \tag{12}$$

Note that $[K]_r$ and $[K]_d$ are the real and artificial matrices consisting of 20×20 and 4×4 elements, respectively. Before applying the transformation, the 20×20 matrix is reconstructed into a 24×24 matrix in order to accommodate the drilling DOF (θ_z) per element. Transformation of the mass matrix is same as that of the stiffness matrix, that is,

$$[\overline{M}] = [\overline{T}]^{\mathrm{T}}[\overline{M}_s][\overline{T}]. \tag{13}$$

3.3. Moving load

In this study, Newmark's explicit integration technique is adopted for the transient analysis of a box girder bridge subjected to the effects of moving loads (Bathe, 1996). Consider a moving load with a velocity v on a plate element. The total moving distance (m) of the load at time $s+\Delta s$ (s) is

$${}^{s+\Delta s}D_s = \frac{v\Delta s}{3.6} + C_{x_2}, \tag{14}$$

where C_{x_2} denotes the initial coordinate of the moving load in the longitudinal direction. The location number $\overline{I}_d$ of the element which the moving load passes through at time $s+\Delta s$ can be expressed as

$${}^{s+\Delta s}\overline{I}_d = N^d_{x_1} I_l + I_s + 1, \tag{15}$$

where

$$I_l = \mathrm{INT}\left(\frac{^{s+\Delta s}D_s N^d_{x_2}}{L_{x_2}}\right), \quad \text{and} \quad I_s = \mathrm{INT}\left(\frac{C_{x_1} N^d_{x_1}}{L_{x_1}}\right). \tag{16}$$

Here, $N^d_{x_1}$ and $N^d_{x_2}$ are the number of division elements in the transverse and longitudinal direction, C_{x_1} is the initial coordinate of the moving load in the transverse direction, L_{x_1} and L_{x_2} are the length of a plate in both directions, and INT( ) means the integer part of value in a parenthesis, respectively.

The moving load vectors $\{F_k(s)\}$ at an arbitrary location on the N^d_kth element of the plate should be inevitably distributed to the nodal loads $\{R_{N_k}(s)\}$ using the Hermite interpolation function $[\Phi]$. The natural coordinates (ξ_k, η_k) of the element for the moving load at time $s + \Delta s$ can be derived as

$$^{s+\Delta s}\xi_k = 2\left(\frac{C_{x_1} N^d_{x_1}}{L_{x_1}} - I_s\right) - 1 \quad \text{and} \quad ^{s+\Delta s}\eta_k = 2\left[\frac{(C_{x_2} + {}^{s+\Delta s}D_s)N^d_{x_2}}{L_{x_2}} - I_l\right] - 1. \tag{17}$$

In a four-node element with 6 degrees of freedom per node, the moving load distributed into four neighborhood nodes can be expressed as

$$^{s+\Delta s}\mathbf{R}_{N_k} = \begin{Bmatrix} S_j \\ S_{j+1} \\ S_{j+2} \end{Bmatrix} = [F_k][I] \begin{Bmatrix} \Phi_j(\xi_k, \eta_k) \\ \Phi'_{j+1}(\xi_k, \eta_k) \\ \Phi''_{j+2}(\xi_k, \eta_k) \end{Bmatrix}, \tag{18}$$

where $j = i + 2$ for $i = 1, \ldots, 3$.

The total magnitude $\boldsymbol{\Theta}$ of the external force applied on the plate at $s + \Delta s$ can be obtained by summing up the distributed N loads as given by

$$^{s+\Delta s}\boldsymbol{\Theta} = {}^{s+\Delta s}\boldsymbol{\Theta}_{N_1} + {}^{s+\Delta s}\boldsymbol{\Theta}_{N_2} + \cdots + {}^{s+\Delta s}\boldsymbol{\Theta}_{N_n}. \tag{19}$$

In Newmark integration scheme the effective loads at time $s + \Delta s$ can be calculated as

$$^{s+\Delta s}\overline{\boldsymbol{\Theta}} = {}^{s+\Delta s}\boldsymbol{\Theta} + [\overline{\mathbf{M}}_s](\lambda_0 {}^s\mathbf{U} + \lambda_2 {}^s\dot{\mathbf{U}} + \lambda_3 {}^s\ddot{\mathbf{U}}). \tag{20}$$

The dynamic displacements $\mathbf{U}$, accelerometers $\ddot{\mathbf{U}}$, and velocities $\dot{\mathbf{U}}$ at time $s + \Delta s$ can be solved as

$$^{s+\Delta s}\mathbf{U} = [\overline{\mathbf{K}}_g]^{-1} {}^{s+\Delta s}\overline{\boldsymbol{\Theta}}, \tag{21}$$

$$^{s+\Delta s}\dot{\mathbf{U}} = \lambda_0({}^{s+\Delta s}\mathbf{U} - {}^s\mathbf{U}) - \lambda_2 {}^s\dot{\mathbf{U}} - \lambda_3 {}^s\ddot{\mathbf{U}}, \quad \text{and} \quad {}^{s+\Delta s}\dot{\mathbf{U}} = {}^s\dot{\mathbf{U}} - \lambda_6 {}^s\ddot{\mathbf{U}} - \lambda_7 {}^{s+\Delta s}\ddot{\mathbf{U}}, \tag{22}$$

where the triangularized effective stiffness matrix is $[\overline{\mathbf{K}}_g] = [\overline{\mathbf{K}}_s] + \lambda_0[\overline{\mathbf{M}}_s]$, λ_0, λ_2, λ_3, λ_6, and λ_7 are integration constants in the Newmark integration method, respectively. A flow chart of the computational procedure considering moving loads is shown in Fig. 3.

4. Numerical results

4.1. Drilling degree of freedom

The finite element formulation for determining the drilling DOF described earlier (Section 3.2) now implemented to compare the results of our technique with those calculated by other investigators. For both static and free vibration analyses, we determine by trial and error process the appropriate stiffness coefficient for the drilling DOF. The additional stiffness does in fact affect the result because it also occurs at

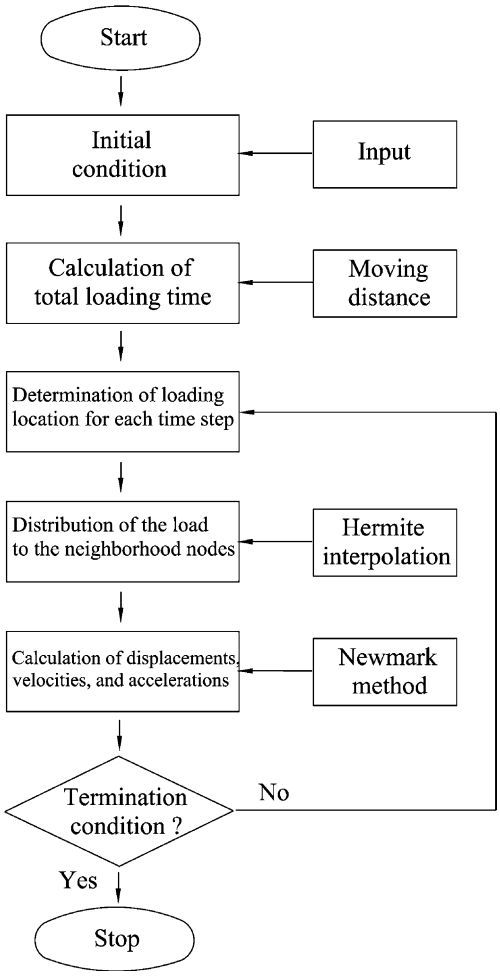

Fig. 3. Flow chart of a numerical dynamic analysis considering moving loads.

nodes which are not co-planar and indeed the device represents an approximation. Therefore the optimal stiffness γ_k should be determined by calculating displacements or natural frequencies for its different values.

Table 1 shows the maximum static vertical displacements of a continuous two-span box girder bridge versus various artificial stiffnesses for the drilling DOF ($\gamma_k = 10^1$–10^{10}). The properties of the box girder bridge are $E = 2.88$ GPa, $v = 0.2$, and $\mu = 2.5$ kN/m^3, respectively. The vehicle has a weight of 24.0 kN for static analysis. For the purpose of comparison, we adopted a finite element package (LUSAS) (Fea Ltd., 1996–2000) which uses a drilling rotational stiffness introduced by Zienkiewicz and Taylors (2000).

Table 1
Maximum static displacements for a continuous two-span box girder bridge for various values of γ_k (cm, LUSAS result = 0.873)

γ_k	10^1	10^2	10^3	10^4	10^5	10^6	10^7	10^8	10^9	10^{10}
Displacement (cm)	1.146	1.145	1.136	1.071	0.946	0.897	0.891	0.891	0.890	0.890
Difference (%)	23.83	23.77	23.14	18.53	7.78	2.92	2.03	1.92	1.91	1.91

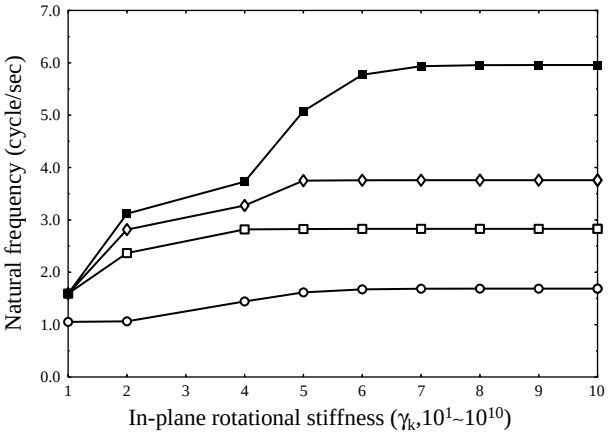

Fig. 4. Natural frequencies for a continuous two-span box girder bridge versus inplane rotational stiffness γ_k. (○) first mode; (□) second mode; (◇) third mode; (■) four mode.

From Table 1, it can be observed that the difference between the results of this study and those of LUSAS is negligible for values of $\gamma_k \geqslant 10^6$.

Fig. 4 shows the natural frequencies of the continuous two-span box girder bridge as a function of various artificial stiffnesses γ_k. The natural frequencies shown in Fig. 4 approach a constant value as the artificial stiffness increases, especially for $\gamma_k > 10^6$. It is interesting to note that the artificial stiffness value of $\gamma_k = 10^6$ is appropriate to minimize the error caused by the drilling DOF for both the static and dynamic analyses. Finally we use stiffness value of 10^6 for the drilling DOF on next stage.

4.2. Dynamic responses for various locations of cross-section

Fig. 5 shows the static and dynamic displacements of $2 \times 60 = 120$ m simply supported box girder bridge subjected to a vehicle moving with the speed of 80 km/h and located at the midpoint of the deck. The properties of the bridge are the same as those described earlier and the moving vehicle has a weight of 24.0 kN. From Fig. 5, it is observed that the dynamic displacements at DT1 and DT5 are noticeably larger than others. In the detailed data, the responses at DT3 and are also slightly larger than those at DT2 and DT4. It may be noted that the dynamic behavior have different characteristics along each locations on the cross-section. In particular, from Fig. 5(a) the induced displacement at midpoint of slab (DT1) is extremely higher than the others because the dynamic response is measured at the surface the loading point. In addition, it may be observed that the displacements near 30.0 m become more dramatic than those at the other loading points because the measuring point is same as the loading point. The one-dimensional analysis using beam elements does not show the dynamic displacements across the cross-section of the box girder bridge. On the other hand, the three-dimensional dynamic analysis using the flat shell elements proposed in this study can determine the dynamic displacement regardless of the locations on the box cross-section. This is a significant contribution of using the folded flat shell elements by enabling taking the detailed analysis of dynamic responses.

Plots of the dynamic magnification factor (DMF) versus load velocity are shown in Fig. 6. It can be observed that the DMF for various locations of the box girder changes from about 1.0 to 1.2 with the variation of velocity (10–120 km/h). The DMF values could be different for the different loads, geometrical shapes of box girder, span length, the number of box cells, velocities of loads, measuring points, etc. In the current American Association of State Highway and Transformation Officials (AASHTO) Standard

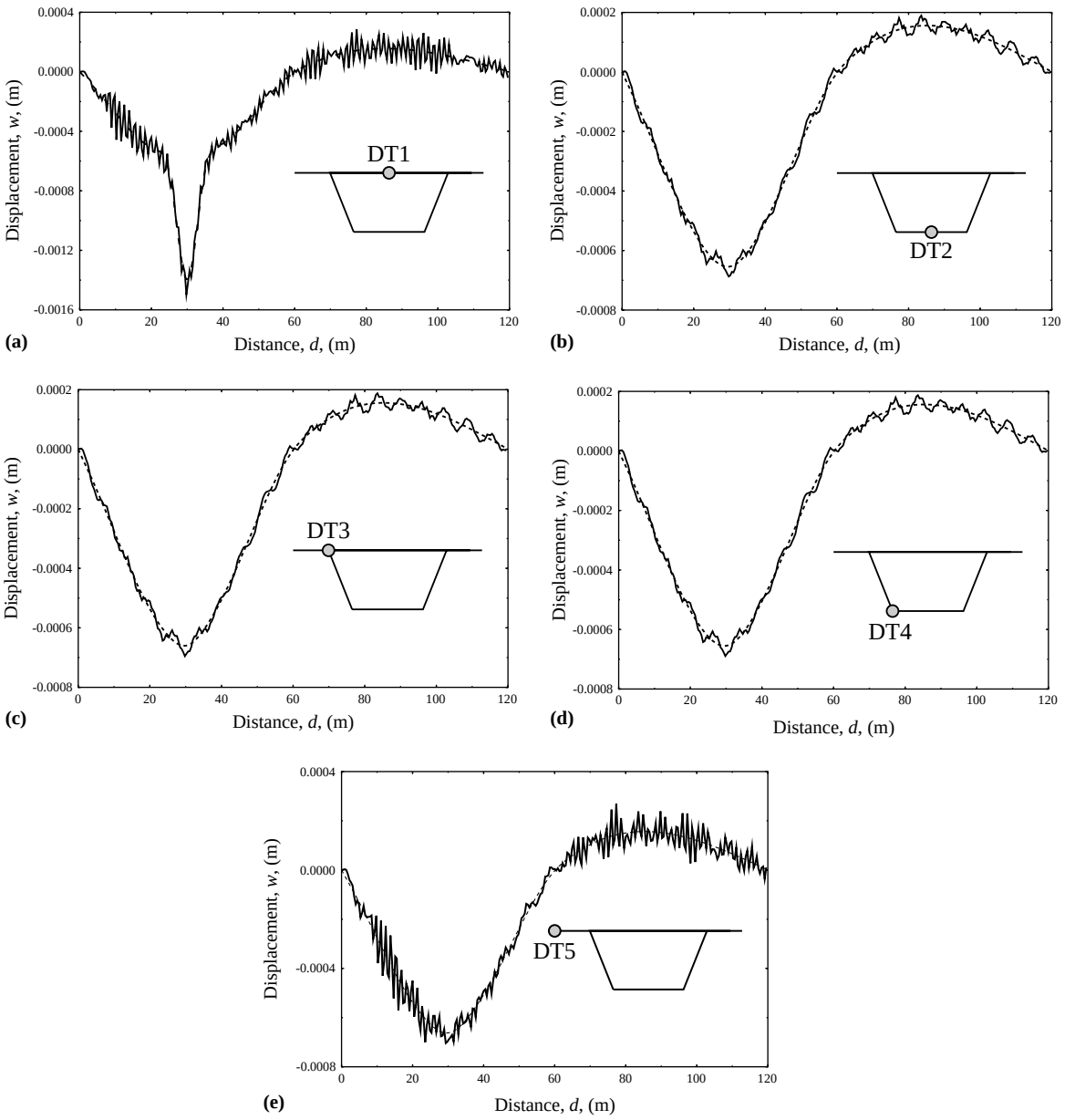

Fig. 5. Dynamic and static deflections of the continuous two-span box girder bridge at various locations on the cross-section: (a) DT1; (b) DT2; (c) DT3; (d) DT4; (e) DT5.

Specifications for Highway Bridges, the dynamic effect is considered through an impact factor (AASHTO, 1996). The impact factor is computed on the basis of span length only. From Fig. 6, it is observed that the DMF for DT5 is about 1.2, which is higher than the value ($\doteq 1.15$) calculated by the specifications. Because the dynamic behavior of a bridge subjected to moving loads depend on the locations across the section, velocity of the moving load, weight of vehicle, and the bridge type, more detailed standards that consider the above mentioned effects of dynamic behaviors are required.

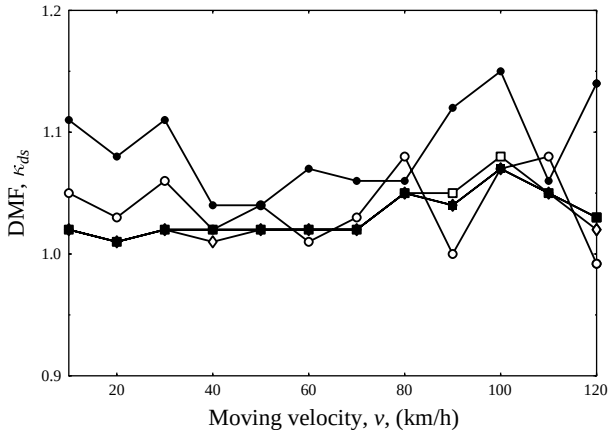

Fig. 6. Dynamic magnification factors of a continuous two-span box girder bridge at various locations on the bridge cross-section. (○) DT1; (□) DT2; (◇) DT3; (■) DT4; (●) DT5.

5. Experimental verification

5.1. Experimental set-up

The finite element formulation described earlier has been implemented to compare the numerical results with the experimental results. In this study, the selected experimental bridge is a newly built long-span bridge across the Han River in Seoul, South Korea. The bridge is designed to sustain heavy traffics of 81,378 crossing vehicles per day. The bridge also consists of typical box sections constructed by incremental launching method (ILM) and free cantilever method (FCM), which is appropriate for the verification of the

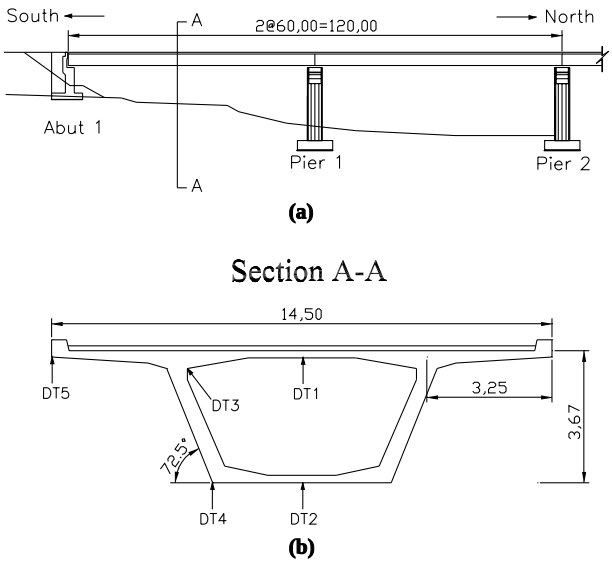

Fig. 7. Elevation and the cross-section of the box girder bridge used for the experimental verification: (a) elevation; (b) cross-section.

finite element program developed in this study. The properties of the concrete for the bridge are the same as those described earlier. The moving vehicle also has a weight of 24.0 kN. Fig. 7 shows the typical cross-section of the experimental bridge and its locations for the measurement. In Fig. 7, DT1–DT5 denote the measuring locations of dynamic responses at the cross-section. Fig. 8 also shows the dynamic test of the box girder under the moving vehicles effects.

5.2. Comparison with numerical results

Fig. 9 shows the comparison between the data obtained from experiments and the numerical results using folded flat shell and beam elements. In Figs. 9 and 10, the location of referred dynamic displacement is at the center point of the span, and the vehicle moves from the starting point to the end point at the center of the bridge deck. As shown in the figures, the results obtained from the experiment are in good agreement with those obtained from the numerical analysis. It can be also observed from the figures that the amplitudes of dynamic response obtained from experiments are somewhat irregular due to external effects such as a roughness of the bridge deck. In addition, the different velocities of the moving load make small influence on the vertical displacements at DT2 and DT3. However, in Figs. 9 and 10, it can be observed that the

Fig. 8. Experimental work for determination of the dynamic response of PSC box bridge subjected to moving vehicles: (a) dynamic test for moving loads; (b) measurement of dynamic deflections.

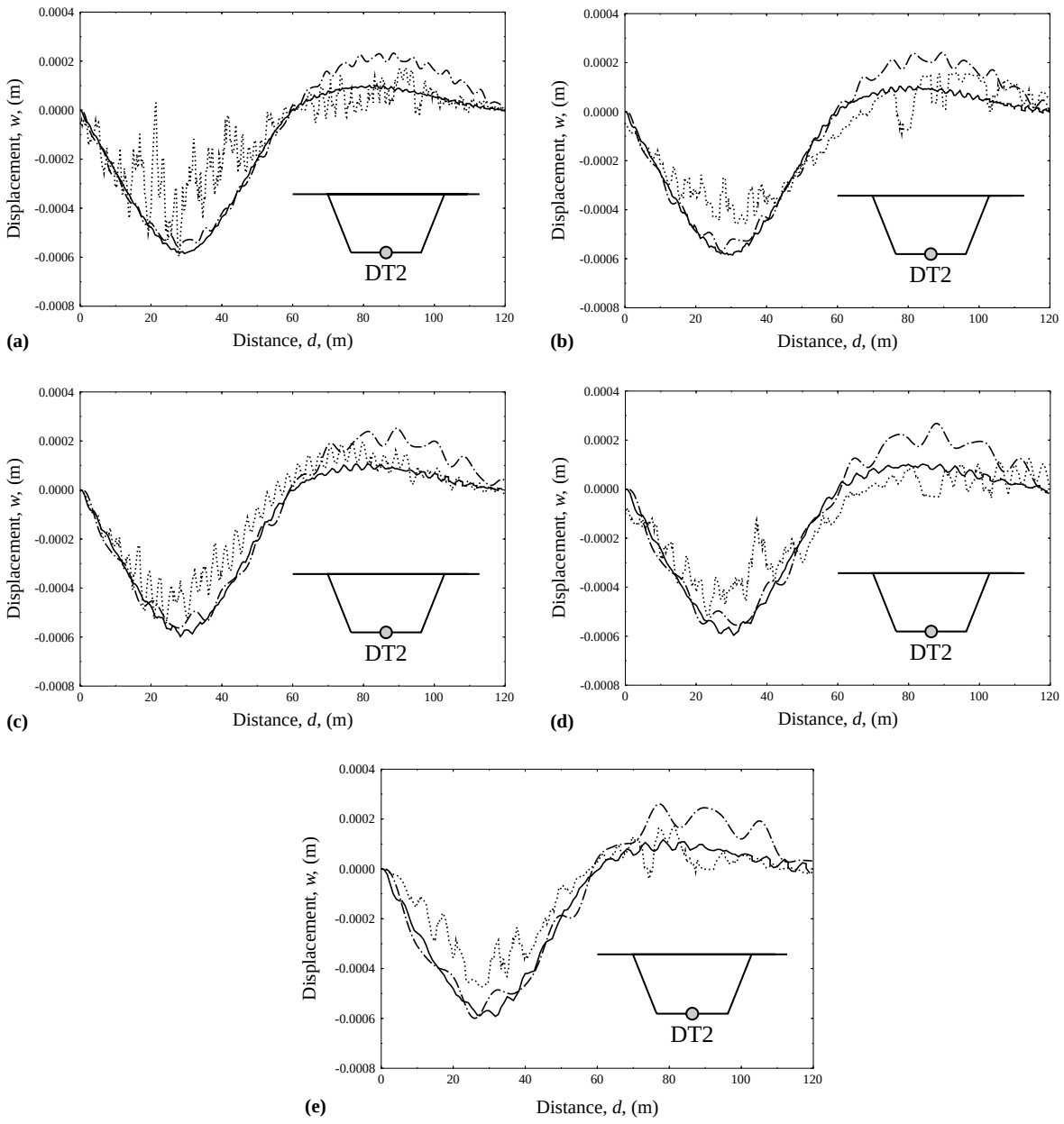

Fig. 9. Dynamic responses at DT2 from experiment, finite element analysis using folded flat shell elements and beam elements for various vehicle speed: (a) 20 km/h; (b) 30 km/h; (c) 40 km/h; (d) 50 km/h; (e) 60 km/h. (—) Folded flat shell elements, (- · -) beam elements, (· · ·) experiment.

frequencies of the dynamic response of our bridge model are significantly different for the different moving velocities. This phenomenon makes sense to us that the increased moving velocity makes greater contribution on the frequency of dynamic response than the vertical displacement.

The displacements using the beam elements were larger than those computed using flat shell element analysis when the moving load is located at the second span of the bridge. It can be observed from the fig-

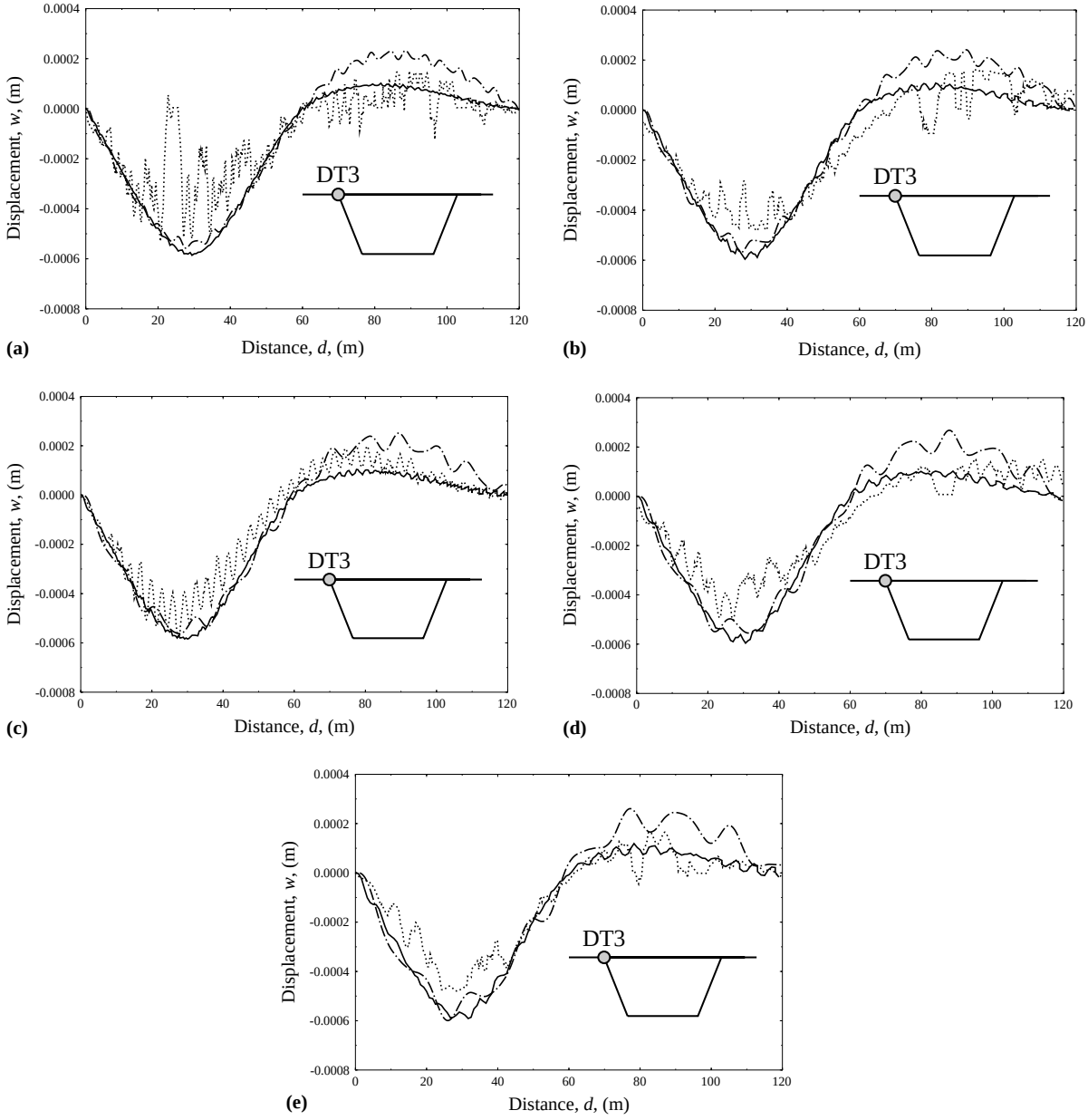

Fig. 10. Dynamic responses at DT3 from experiment, finite element analysis using folded flat shell elements and beam elements for various vehicle speed: (a) 20 km/h; (b) 30 km/h; (c) 40 km/h; (d) 50 km/h; (e) 60 km/h. (—) Folded flat shell elements, (- · -) beam elements, (· · ·) experiment.

ures that the differences in maximum displacement vary from about 10% to 15% from experimental data. In the one-dimensional dynamic analysis using the existing beam element, it is not possible to determine separately from DT1 to DT5. On the other hand, the three-dimensional dynamic analysis using the flat shell element can determine the dynamic displacement for all locations of the box section. Therefore, the dynamic analysis using the flat shell element plays a major role in determining the displacements which are

analogous to the real behavior of the box girders. As we described earlier, since many of the highway bridges are deteriorating due to faster vehicles and overloading, more accurate dynamic analysis standards which consider various factors for highway bridges are required.

6. Summary and conclusion

In this paper, a dynamic analysis using folded flat shell elements is carried out to study the dynamic behaviors in various locations of a continuous two-span box girder bridge subjected to moving loads. For the numerical analysis, we developed a finite element computer program using 6 degrees of freedom per a node for the box girder bridge considering moving load effects. In order to verify the numerical analysis, we have carried out dynamic experiments for real structures, and the results obtained were in good agreement with those computed using the numerical methods. The dynamic characteristics of a two-span box girder bridge subjected to moving loads are analyzed by considering various parameters, especially at different locations across the cross-section. The current standard specifications for highway bridge is not enough to determine accurately the complicated dynamic effects for long-span box girder bridges. In particular, because the dynamic behavior of a bridges subjected to moving loads depend on the locations across the section, velocities of moving load, weight of vehicles, and the bridge type, more detailed standards that consider such various factors are required. It may be concluded from this study that the dynamic effects for different locations on the cross-section, largely governing the behavior of box girder structures subjected to moving loads, should not be neglected and thus the three-dimensional models using folded flat shell elements should be used to analyze such structures for better accuracy.

References

AASHTO 1996. Standard Specifications for Highway Bridges, 17th Ed., Washington, DC.

Bathe, K.J., 1996. The Finite Element Procedures in Engineering Analysis. Prentice Hall, New Jersey.

Biggs, J.M., 1959. Vibrations of simple span highway bridges. Transactions, American Society of Civil Engineers 124.

Chatterjee, P.K., Datta, T.K., Surana, C.S., 1994. Vibration of suspension bridges under vehicular movement. Journal of Structural Engineering, American Society of Civil Engineers 120, 681–703.

Cheung, Y.K., 1969. Folded plate structures by finite strip method. Journal of Structural Engineering, American Society of Civil Engineers 95, 2963–2979.

Cheung, M.S., Li, W., Chidiac, S.E., 1996. Finite Strip Analysis of Bridges. E&FN Spon, an imprint of Chapman & Hall, London, UK.

Chu, K.H., Garg, V.K., Wang, T.L., 1986. Impact in railway prestressed concrete bridges. Journal of Structural Engineering, American Society of Civil Engineers 112, 1036–1051.

Fea Ltd., 1996–2000. Theory Manual Vol. I, II, LUSAS, London.

Hwang, E.S., Nowark, A.S., 1991. Simulation of dynamic load for bridges. Journal of Structural Engineering, American Society of Civil Engineers 117, 1413–1434.

Jeffcott, H.H., 1929. On the vibrations of beam under the action of moving loads. Philosophical Magazine, Series 7 8, 66–97.

Lee, R.C., Lee, S.Y., Yhim, S.S., 2002. A study on the dynamic responses of PSC box girder bridge under the moving load. In: Proceedings of the First International Conference on Bridge Maintenance Safety and Management, Barcelona.

Looney, C.T.G., 1958. Hi-speed computer applied to bridge impact. In: Proceedings of the American Society of Civil Engineers, vol. 84, ST5.

Lowan, A.N., 1935. On transverse oscillations of beams under the action of moving variable loads. Philosophical Magazine, Series 7 19, 708.

Maleki, S., 1991. Compound strip method for box girders and folded plates. Computers and Structures 40, 527–538.

Senthilvasan, J., Thambirtnam, D.P., Brameld, G.H., 2002. Dynamic response of a curved bridge under moving truck load. Journal of Engineering Structures 24 (10), 1283–1293.

Stokes, G.G., 1849. Discussion of a differential equation related to the breaking of railway bridges. Transaction of the Cambridge Philosophical Society 8, 707–735.

Thambiratnam, D.P., Brameld, G.H., Memory, T., 2000. Experimental analysis of an asymmetric reinforced concrete bridge under vehicular loads. Journal of Structural Engineering and Mechanics 9 (1), 17–35.

Timoshenko, S.P., 1922. On the forced vibration of bridges. Philosophical Magazine, Series 6 43, 1018–1019.

Veletsos, A.S., Huang, T., 1970. Analysis of dynamic response of highway bridges. Journal of Engineering Mechanics Division, American Society of Civil Engineers 96, 593–620.

Willis, R., 1849. Appendix to the Report of the Commissioners Appointed to Inquire into the Application of Iron to Railway Structures. H.M. Stationary Office, London, UK.

Yang, Y.B., Yau, J.D., 1997. Vehicle-bridge interaction element for dynamic analysis. Journal of Structural Engineering, American Society of Civil Engineers 123, 1512–1518.

Zienkiewicz, O.C., Taylors, R.L., 2000. The Finite Element Method Volume II: Solid Mechanics. B.H. Publications, pp. 225–243.